Nano Energy 102 (2022) 107672

Contents lists available at ScienceDirect

Nano Energy

journal homepage: www.elsevier.com/locate/nanoen

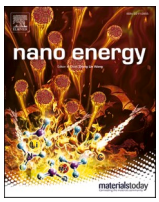

Rational design of air-stable and intact anode-electrolyte interface for garnet-type solid-state batteries

Jiaxu Zhang [a,1], Changhong Wang [b,1], Matthew Zheng [b], Minghao Ye [a], Huiyu Zhai [a], Jun Li [a], Gangjian Tan [a,*], Xinfeng Tang [a,*], Xueliang Sun [b,*]

[a] State Key Laboratory of Advanced Technology for Materials Synthesis and Processing, Wuhan University of Technology, Wuhan 430070, China
[b] Department of Mechanical and Materials Engineering, University of Western Ontario, 1151 Richmond St., London, Ontario N6A 3K7, Canada

ARTICLE INFO

Keywords:
Air-stability
Li-deficiency
Garnet electrolytes
Solid-state batteries

ABSTRACT

Garnet-type solid-state electrolytes are a promising fast lithium-ion conductor due to their high room-temperature ion conductivity and inherent stability against lithium metal. However, interfacial lithiophobic Li_2CO_3 makes garnet/Li interfacial ionic contact challenging. The general approach to physically or chemically eliminating Li_2CO_3 inevitably leads to a Li-deficiency layer at the garnet surface, significantly retarding interfacial ion transport. Contrary to the aforementioned approach, herein we chemically upcycle the Li_2CO_3 on the garnet surface *via* the double replacement reaction between Li_2CO_3 and SiO_2. This approach in-situ constructs an air-stable and lithiophilic Li_xSiO_y (LSO) on the garnet surface and averts the Li-deficiency layer formation. The LSO modified symmetric cell displays a low interfacial impedance of 3 Ω cm^2 and a high critical current density of 1.2 mA cm^{-2} at 30 ^{0}C. This work provides a promising strategy to upcycle interfacial Li_2CO_3 on the garnet electrolyte.

1. Introduction

Since lithium-ion batteries (LIBs) were commercialized in 1991, there has been an increasing interest in the energy storage sector [1]. Nevertheless, the current LIBs cannot meet future consumer requirements for energy density and safety due to the rapid advancement of energy storage technology [2]. Li-metal batteries have attracted much attention due to their extremely high energy density [3,4]. However, the safety risks (leakage and deflagration) stemming from lithium dendrites inevitably hamper the application of the Li metal anode [5]. Recently, many strategies have been reported to address the problem, for instance, forming a protective layer on lithium metal, [6,7] designing electrolyte solvents, [8] homogenizing current density by creating porous current collectors, [9] and using solid-state electrolytes (SSEs) [10]. Among these, the ultimate alternative solution is to use non-toxic and non-flammable SSEs instead of liquid electrolytes to develop all-solid-state lithium batteries (ASSLBs) [11].

Various SSEs have been developed to enable ASSLBs [12–19]. Among them, cubic garnet-type $Li_7La_3Zr_2O_{12}$ (LLZO) is outstanding because of its wide electrochemical window, excellent chemical stability against lithium metal, and high room-temperature ionic conductivity *via* aliovalent ion doping [20]. However, the poor interfacial wettability between Li metal anode and garnet has significantly hindered its application in ASSLBs [21]. Since garnet is naturally lithiophilic, [22] the poor interfacial wettability is generally attributed to the spontaneously formed Li_2CO_3 on its surface during air exposure *via* ion exchange, [23] single-step reactions, [24] or hydration reaction [25]. The lithiophobic Li_2CO_3 layer leads to inhomogeneous Li^+ transfer across the interface and thus huge interfacial resistance [26,27].

Some strategies have been proposed to improve interfacial ionic contact, which can be approximately classified into three categories: "concealing", "eliminating", and "transforming". "Concealing" represents designing a lithiophilic layer to cover the surface of LLZO [28–32]. However, the Li_2CO_3 on the surface of LLZO is not eradicated, which effectively destroys the Li/LLZO interface stability [33,34]. "Eliminating" means directly removing the surface Li_2CO_3 from garnet. For instance, surface polishing and high-temperature pulsing can physically remove the Li_2CO_3 [22,35]. However, Li_2CO_3 is only provisionally removed. When the treated electrolyte pellets are re-exposed to air, Li_2CO_3 regenerates quickly. Carbothermal treatment and acid corrosion

* Corresponding authors.
E-mail addresses: gtan@whut.edu.cn (G. Tan), tangxf@whut.edu.cn (X. Tang), xsun9@uwo.ca (X. Sun).
[1] These authors contributed equally.

https://doi.org/10.1016/j.nanoen.2022.107672
Received 21 May 2022; Received in revised form 21 July 2022; Accepted 2 August 2022
Available online 4 August 2022

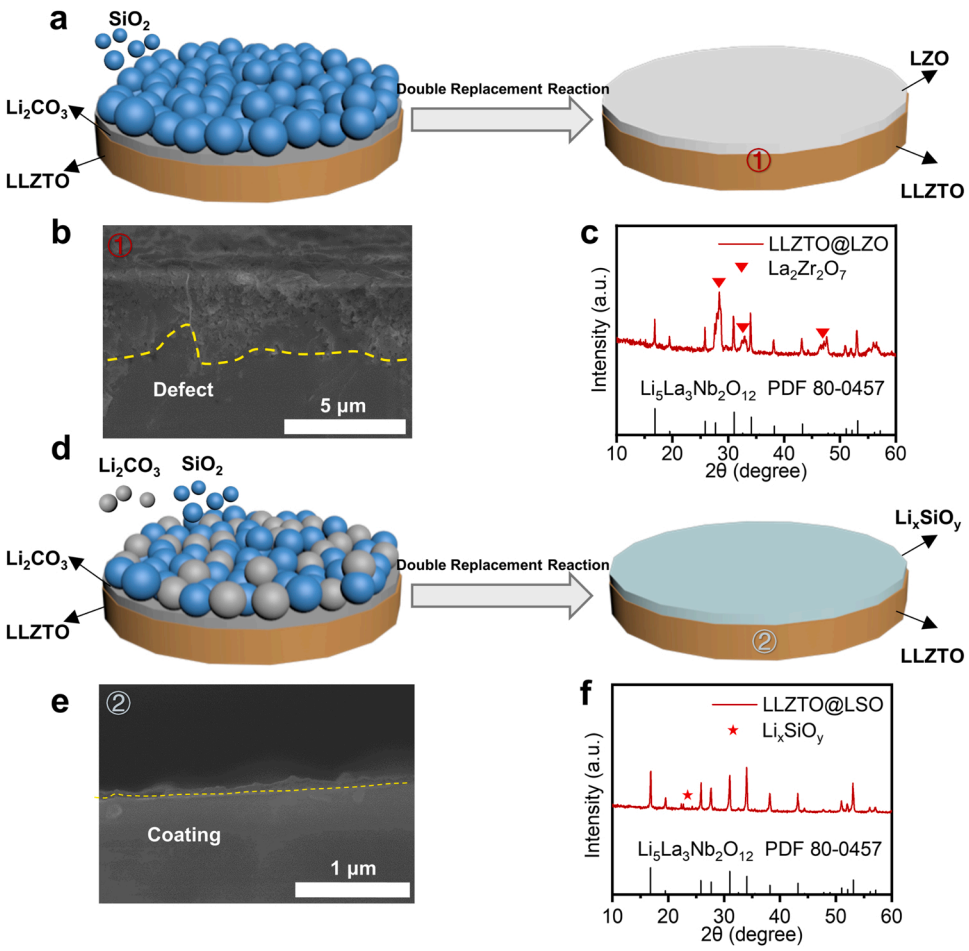

Fig. 1. (a) Schematic illustration of the preparation process of LLZTO pellet reacted with SiO_2 powders (The treated pellet is denoted as LLZTO@LZO). (b) Cross-section SEM image of the LLZTO@LZO pellet. (c) XRD patterns of LLZTO@LZO pellet. (d) Schematic illustration of the preparation process of LLZTO pellet reacted with Li_2CO_3 and SiO_2 powders mixed in a mole ratio of 1:1 (The treated pellet is denoted as LLZTO@LSO). (e) Cross-section SEM image of LLZTO@LSO pellet. (f) XRD patterns of LLZTO@LSO pellet.

are strategies to remove the Li_2CO_3 chemically [36–38]. Nevertheless, the chemical reaction should be carefully controlled to prevent the structural degradation of LLZO. "Transforming" means converting Li_2CO_3 into a lithiophilic surface layer. Fluorinated or silicated lithium layers have been successfully converted [39,40]. Interestingly, the formation of Li_2CO_3 consumes lithium from LLZO. In other words, the elimination or transformation of Li_2CO_3 inevitably leads to Li-deficiency defects at the interface in all the methods mentioned above. This Li-deficient layer aggravates lithium dendrite formation, especially under high current densities [41–44]. Therefore, cleaning the surface Li_2CO_3 and spontaneously constructing an air-stable without Li-ion deficiency layer is significant to the garnet interface design.

In this work, we design an effective strategy to chemically convert the detrimental Li_2CO_3 into lithiophilic Li_xSiO_y (denoted as LSO hereafter) and simultaneously prevent the formation of Li-deficiency defects through a double replacement reaction between Li_2CO_3 and SiO_2. As a hydrophobic material, the air-stable LSO layer prevents surface Li_2CO_3 regeneration upon exposure to moisture. Meanwhile, LSO is proven to be lithiophilic. The excellent interface wettability leads to intimate interfacial ionic contact between Li metal and garnet pellets. Compared with Li_2CO_3, LSO has higher voltage stability (decomposition voltage over 4.5 V) and ion conductivity ($\sigma_{Li}^{+} = 5.6 \times 10^{-7}$ S cm^{-1} at 25 ℃), which leads to fast interfacial ion-exchange current and high interfacial stability between Li metal and garnet SSEs [21,39]. As a result, a garnet-based Li symmetric cell demonstrates a low interfacial impedance of 3 Ω cm^2 and a high critical current density of 1.2 mA cm^{-2} at 30 ^{0}C. This work provides new insight into the interface design of garnet SSEs.

2. Materials and methods

2.1. Preparation of garnet electrolyte pellets

The $Li_{6.4}La_3Zr_{1.4}Ta_{0.6}O_{12}$ (99.99% purity, denoted as LLZTO) were purchased from Kejing Incorporation (MTI, Hefei, China). Li_2CO_3 powders (99.99% purity) were purchased from Sigma-Aldrich. SiO_2 powders (99.99% purity) were purchased from Inno-Chem. All the materials in this work were used without further purification. Firstly, the LLZTO powder was loaded into Φ12.5 mm graphite dies and densified by a hot press machine at 1150 ^{0}C for 1 h under an axial pressure of 20 MPa in Ar atmosphere. Then the sintered pellet was polished manually with sandpaper to obtain a flat surface. The polished LLZTO pellet was exposed to air for a week to age. Li_2CO_3 and SiO_2 powders (in a mole ratio of Li_2CO_3/SiO_2 =1/1, 2/1 or 0/1) were thoroughly ground in an agate mortar with isopropanol and dried at 80 ^{0}C for 0.5 h. Then the mixtures (1 g) were used to coat both sides of the LLZTO pellet, and the coated LLZTO pellet was heated at 750 ^{0}C for 10 min in Ar atmosphere. After that, the mixtures were blown away from the top and bottom of the pellet.

2.2. Characterizations

The X-ray Diffraction (XRD; PAN analytical–Empyrean) with a Cu Kα was used to confirm the crystal structure and phase composition of the as-prepared LLZTO and LLZTO@LSO pellets. The morphology and elemental distribution were characterized using field emission scanning electron microscopy (FESEM; Hitachi SU8020) coupled with an energy-dispersive X-ray (EDS). Raman spectroscopy (RENISHAW InVia) was

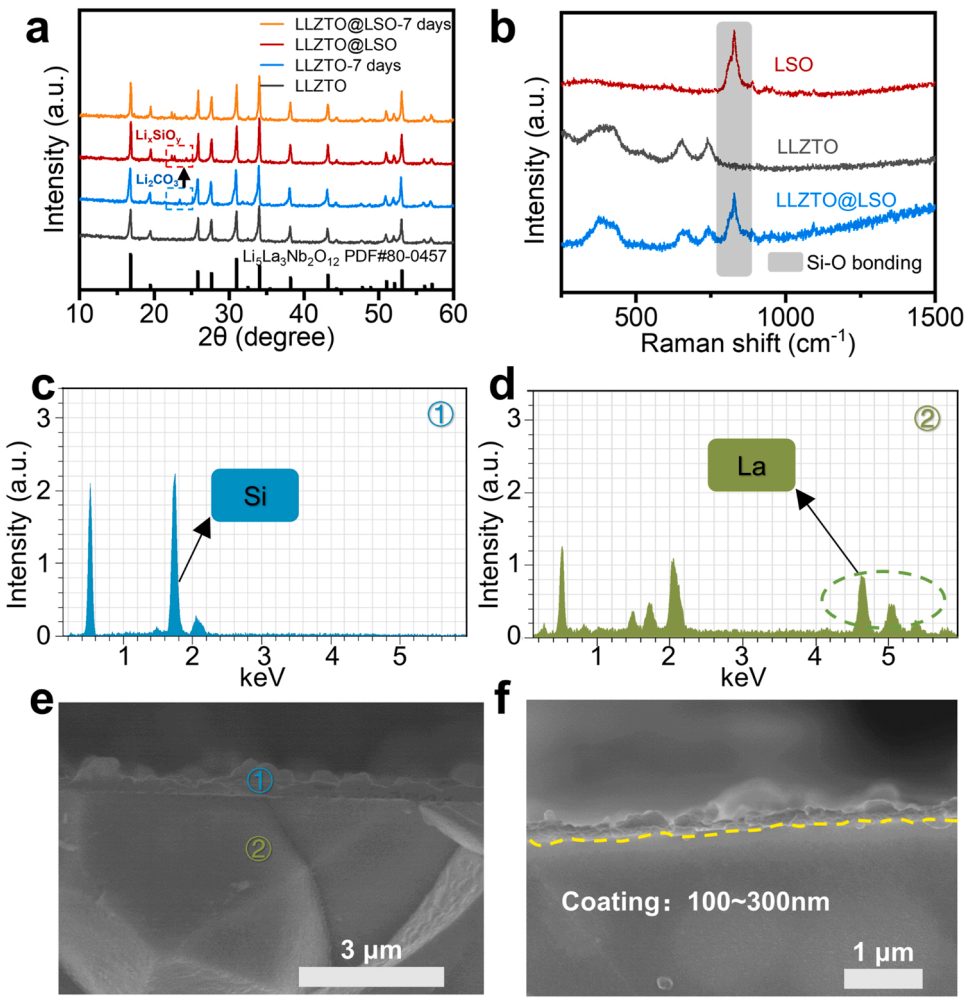

Fig. 2. Structure and phase characterization of the LLZTO@LSO and LLZTO pellet. (a) XRD patterns of LLZTO, LLZTO@LSO pellet and after exposing them to air for 7 days. (b) Raman spectra of prepared LSO powders, LLZTO@LSO pellet, and LLZTO pellet. (c, d) EDS analysis corresponds to points 1 and 2 in the SEM image of (e). (e, f) Cross-section SEM image of the LLZTO@LSO pellet.

performed with a 623.8-nm argon-ion laser.

2.3. Cell fabrications and electrochemical performance tests

All the preparation processes for the cell were conducted in a glove box filled with ultra-pure argon to avoid alteration of lithium metals. Fresh lithium disks were cut from a lithium block and pressed homogeneously in thickness for use. For a typical Li/LLZTO@LSO/Li symmetrical cell assembly, the LLZTO@LSO pellet was firstly sandwiched by two fresh lithium disks and pressed slightly by hand. Then they were subject to heat treatment on a hot plate at 200 ^{0}C for 30 min. After cooling to room temperature, the sandwich cell was carefully sealed in a battery shell (CR 2032). The Li/LLZTO/Li symmetric cell was assembled with the same procedure.

The hybrid-state full cell was fabricated as follows. Firstly, the commercial $LiFePO_4$ (MTI, Hefei, China), Ketjenblack (MTI, Hefei, China), and Polyvinylidene fluoride (MTI, Hefei, China) were thoroughly mixed at a mass ratio of 8:1:1 and coated on clean Al foil homogeneously. After drying at 120 ^{0}C overnight, the Al foil was punched into discs with a mass loading of ~1.8 mg·cm^{-2} and stored in the glove box. One side of the prepared LLZTO@LSO pellet was compacted by a lithium disc and heated at 200 ^{0}C for 30 min. On the other side, after polishing the LSO layer, a tiny amount of liquid electrolyte (1.0 M $LiPF_6$ in EC:DMC:EMC = 1:1:1 vol%, ~ 10 μl) was added to wet the pellet/cathode interface. Then they were sealed carefully into a battery shell.

Blocking electrodes were coated with sputtering gold onto both sides of the electrolyte pellets (1.5 min sputter time, VTC-16-D Sputter-Coater) before the conductivity test. Using a BioLogic VSP-300 electrochemical station, the Electrochemical impedance spectroscopy (EIS) of the symmetric cells was measured with an alternating current (AC) amplitude of 10 mV from 1 to 7 × 10^6 Hz in frequency. The electrochemical performance of the symmetric and full cells was evaluated by the Land CT2001A battery test system at 30 ^{0}C. Galvanostatic stripping−plating cycling was conducted to test the ion transportability across interfaces. And galvanostatic charge/discharge tests were conducted at various current densities between 2.8 and 4.2 V.

3. Results and discussion

A cubic garnet electrolyte with nominal compositions of $Li_{6.4}La_3Zr_{1.4}Ta_{0.6}O_{12}$ (LLZTO) is used for this study. It has been reported that the double replacement reaction between Li_2CO_3 and SiO_2 is feasible above the melting point of Li_2CO_3 (723 ^{0}C), and the desired Li_xSiO_y forms easily [39]. Considering the existence of Li_2CO_3 on the surface of the air-aged LLZTO pellet, a proper amount of SiO_2 powders was directly coated on the surface of the LLZTO pellet. Then the coated pellet was subjected to heat treatment, as shown in Fig. 1a. After the reaction, the powders on the surface of the treated pellet were blown away. However, the cross-sectional scanning electron microscopy (SEM) indicates that a defect layer (2–4 μm) exists near the surface of the

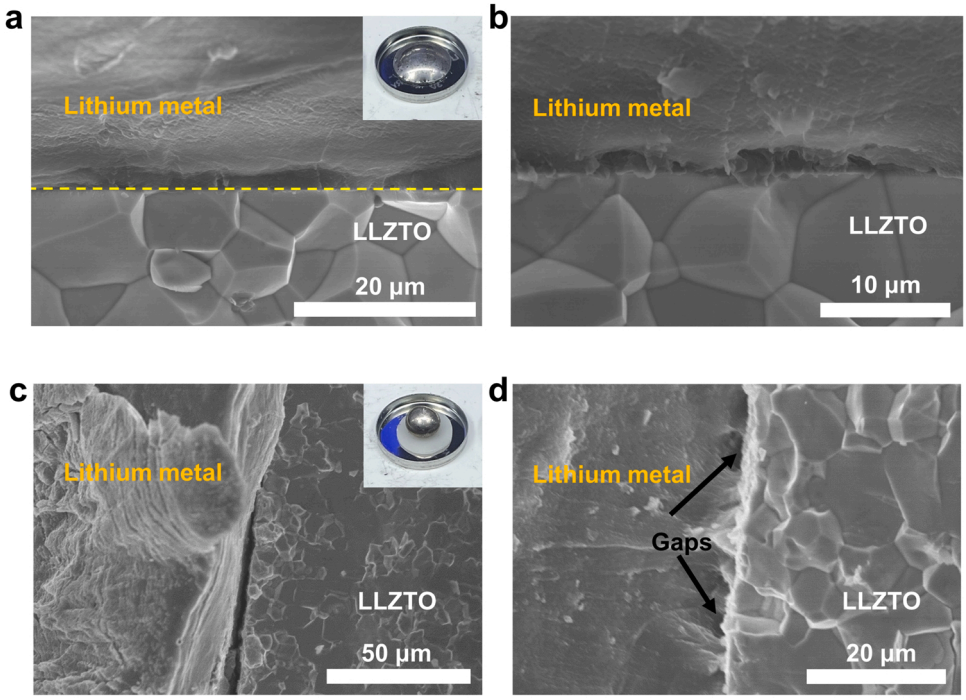

Fig. 3. (a, b) SEM images of interfaces between Li metal and LLZTO@LSO pellet. The wetting behavior between molten Li metal and LLZTO@LSO pellet was shown in the inset of (a). (c, d) SEM images of interfaces between Li metal and LLZTO pellet. The wetting behavior between molten Li metal and LLZTO pellet was shown in the inset of (c).

LLZTO pellet (Fig. 1b and S1). X-ray diffraction (XRD) analysis confirms that a Li-deficiency phase ($La_2Zr_2O_7$, PDF # 71–2363, denoted as LZO hereafter) is formed at the interface (Fig. 1c). In addition, the formation of LZO can be confirmed by Raman results [52], Fig. S7. The formation of LZO is due to the Li_2CO_3 on the surface of LLZTO completely reacting with SiO_2. The superfluous SiO_2 will strip lithium from the LLZTO. A similar phenomenon is also observed in previous reports [45,46]. As a kind of Li ionic insulator, LZO significantly reduces the ion conductivity of the garnet electrolyte, and Li-ions easily combine with electrons here to aggravate lithium dendrite [41–44]. To avoid the formation of LZO, we added extra Li_2CO_3 and mixed it with SiO_2 powders in a mole ratio of 1:1. The mixtures were then coated on the surface of the LLZTO pellet, which was later subjected to the same process mentioned above. Thanks to extra Li_2CO_3, the anticipative LSO was successfully coated on the surface of LLZTO without the formation of LZO, as schematically illustrated in Fig. 1d. The LSO coating layer was confirmed by cross-sectional SEM in Fig. 1e. Furthermore, the XRD patterns also indicate the formation of LSO (PDF # 004–0727, 004–0436), Fig. 1f. This treated pellet is named LLZTO@LSO. In addition, we tried mixing Li_2CO_3 and SiO_2 powders in a mole ratio of 2:1 as the coating mixtures, but the generated coating layer is too thick (~2 μm), which may hinder the Li-ion across the interface, Fig. S2.

As shown in Fig. 2a, all the prepared LLZTO pellet diffraction patterns are in agreement with the cubic structured $Li_5La_3Nb_2O_{12}$ (PDF # 80–0457). After exposing the LLZTO pellet to air for 7 days, additional sharp peaks associated with Li_2CO_3 emerge at 23^0, indicating the spontaneous formation of Li_2CO_3 on the garnet surface during air exposure [47]. Finally, the Li_2CO_3 was successfully transformed into the LSO through our strategy. Accordingly, the peaks of Li_2CO_3 vanish, and the peaks associated with LSO emerge at around 22^0 and 24^0 (PDF # 004–0727, 004–0436). Furthermore, after exposing the LLZTO@LSO pellet to air for a week, prominent peaks associated with Li_2CO_3 are not revealed. This unambiguously points towards the air stability of the LLZTO@LSO pellet. Meanwhile, the Raman-active vibrational modes of the LLZTO@LSO pellet, LLZTO pellet, and the synthetic LSO powders were detected by the Raman spectra, Fig. 2b. For the LLZTO and LLZTO@LSO pellet, notable peaks emerging at 380, 421, 656, and 742 cm^{-1} are detected. The peak s at 380 cm^{-1} and 421 cm^{-1} are attributed to the Li-O bonding, and the latter two represent the stretching of Zr−O and Ta−O bonding, respectively [37,48]. And the peak at 826 cm^{-1} for the LLZTO@LSO is consistent with the LSO powders, which is assigned to the Si-O bonding vibration model [49,50]. To further prove the existence of the LSO layer, SEM and energy-dispersive X-ray spectroscopy (EDS) analysis of the LLZTO@LSO pellet are conducted, as shown in Fig. 2c-f. The EDS analysis of the coating layer indicates the presence of silicon (point 1 in Figs. 2c and 2e), which is the constituent element of LSO. Combined with the XRD and Raman results, the layer can be confirmed as LSO, which is 100 ~ 300 nm thick and has good contact with garnet pellet, Figs. 2e and 2f. The LLZTO bulk was also detected (point 2 in Figs. 2d and 2e), and the typical La signal was marked. It should be noted that the Ta element signal (emission line 1.709 eV for Mα1-shell) overlaps with the Si element signal (emission line 1.739 eV for Kα1-shell) [51]. Hence, the weaker signal peak around 1.7 eV observed in point 2 (the LLZTO bulk) may attribute to the Ta element, and the more substantial signal peak observed in point 1 (the coating layer) should attribute to the Si element. The inside bulk morphology of LLZTO and LLZTO@LSO were also observed by cross-sectional SEM (Fig. S3). Both display compact and large grains, which coincide with their high relative density (over 99% of theoretical ones) by the Archimedes method. Combined with the XRD patterns of LLZTO@LSO and LLZTO, this confirms that the external LSO layer does not alter the garnet bulk structure.

Transforming Li_2CO_3 into LSO on the surface of the LLZTO pellet greatly improves the wettability of garnet electrolyte pellet with Li metal. In the case of LLZTO@LSO, molten lithium metal spreads out quickly and wets the entire electrolyte surface, as shown in the inset of Fig. 3a. As such, it creates an exceptionally intimate and tight contact at the electrolyte and Li metal interface, and no gaps are observed from the cross-sectional SEM in Figs. 3a and 3b. To investigate how the LSO layer combines with lithium metal, the prepared LSO powders were mixed with molten lithium metal at 200 ^{0}C. As shown in Fig. S4, LSO powders were easily mixed with molten lithium metal. After cooling to room

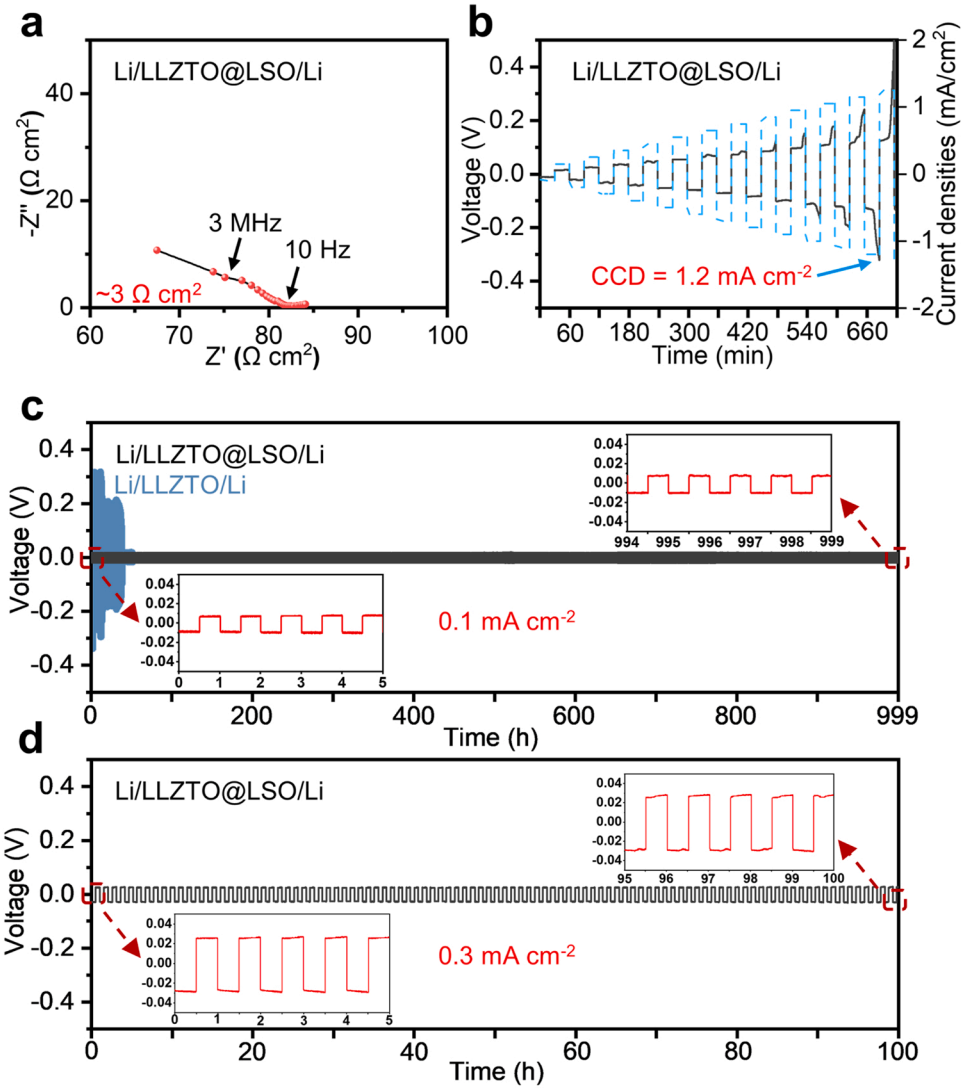

Fig. 4. Electrochemical characterization of the symmetric cells. (a) EIS measurements of the Li/LLZTO@LSO/Li symmetric cells. (b) Polarization curve of the symmetric cell at different current densities (30 min for per plating or stripping). (c, d) Polarization curve of Li/LLZTO@LSO/Li, Li/LLZTO/Li symmetric cell during the long-term striping-plating process (1 h for a per-cycle) at a current density of (c) 0.1, and (d) 0.3 mA·cm^{-2}. Insets show the magnifying curves at different times during the cycle process.

temperature, XRD was performed on the LSO/Li mixture (Fig. S5). Except for the peaks related to LSO and Li metal, no other apparent peaks are found, indicating that they combine physically and no severe chemical reaction occurred. In contrast, for the LLZTO pellet, the molten lithium metal exhibits a high contact angle, like a dewdrop on a lotus leaf, inset of Fig. 3c. The "lotus effect" that occurred on the surface of the LLZTO pellet is indicative of poor wettability with Li metal, because the Li_2CO_3 layer on the surface of LLZTO is naturally lithiophobic. Hence, there are loose contact and significant gaps between Li metal and LLZTO pellet as observed by SEM, Figs. 3c and 3d.

Li/LLZTO@LSO/Li and Li/LLZTO/Li symmetric cells were assembled and tested at 30 ^{0}C. Firstly, electrochemical impedance spectroscopy (EIS) was conducted to evaluate the charge transfer resistance at the Li/LLZTO@LSO and Li/LLZTO interfaces. The impedance spectroscopy in the high frequency should be mainly attributed to the bulk resistance because the Li^+ response frequency is much higher at bulk (the grain and grain boundary of electrolyte) than that of the interface between Li metal and electrolyte. Accordingly, as shown in Fig. S6, the bulk resistance of the electrolyte equals the left intercept of semi-circle at high frequency from the Nyquist plots, which is ~114 ohm·cm^2. Moreover, the total resistance of the symmetric cell equals the left intercept of semi-circle at medium frequency, which is 2715 ohm·cm^2. After subtracting the bulk resistance from the total, the interfacial resistance in Li/LLZTO is calculated to be ~1300 ohm·cm^2, which is the half distance of the intercept between the semi-circle at high and medium frequencies. For Li/LLZTO@LSO/Li symmetric cell, Fig. 4a. The semicircle in the Nyquist plot characterizes the electrode/electrolyte interface (from ~75 ohm·cm^2 to ~81 ohm·cm^2). Considering the two Li/LLZTO interfaces, the Li/LLZTO interfacial resistance is calculated to be ~3 ohm·cm^2. The significant decrease in interfacial resistance stems from the seamless and enhanced Li/LLZTO@LSO interface.

We further tested the critical current density and overpotential of Li/LLZTO@LSO/Li symmetric cells under step-increased current densities. As shown in Fig. 4b, the overpotential response remains steady until the current density reaches to 0.95 mA cm^{-2}. Above that, the overpotential becomes slightly steep, and the abrupt voltage fluctuation appears at the current density of 1.25 mA cm^{-2}, indicating a short-circuit phenomenon. The large CCD in Li/LLZTO@LSO/Li symmetric cell is ascribed to enhanced interfacial contact and uniform Li^+ flux after *in-situ* transforming the Li_2CO_3 to LSO layer. To indicate the electrochemical stability of the Li/LLZTO@LSO interface, the lithium plating−stripping cycling performance of symmetric cells was tested at different current densities. Each plating or stripping period was sustained for 30 min. At the current density of 0.1 mA cm^{-2}, Fig. 4c, the cell can steadily cycle for 999 h with almost identical overpotential plateaus of 12.1 mV. In contrast, Li/LLZTO/Li symmetric cell break down for ~38 h. In addition, at the current density of 0.3 mA cm^{-2}, the overpotential plateaus are still steady all the time and display a small voltage hysteresis of

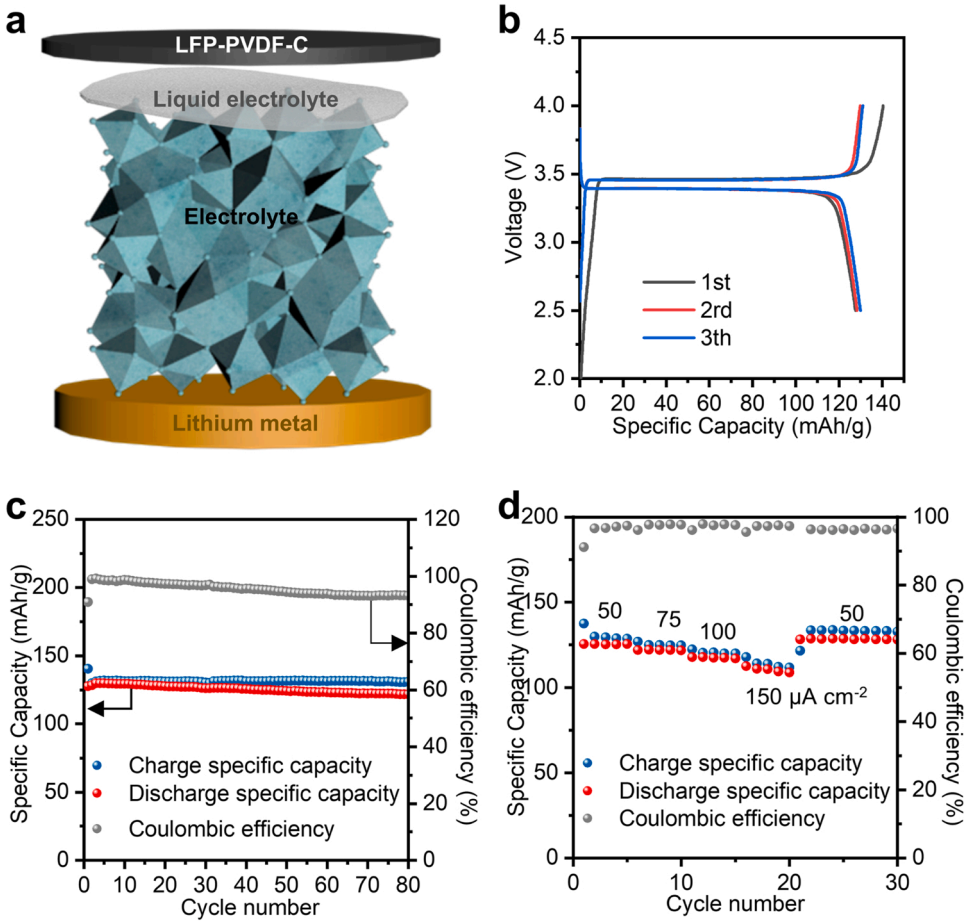

Fig. 5. Electrochemical performance of hybrid solid-state full cells. (a) A proof-of-concept demonstration of the assembled Li/LLZTO@LSO/LFP hybrid solid-state cell. (b) Charge and discharge profiles of the hybrid solid-state cell for the first three cycles at a current density of 50 μA cm^{-2}. (c) Cycling performance of the hybrid solid-state cell at a current density of 50 μA cm^{-2}. (d) Rate performance of the hybrid solid-state cell at different current densities.

26.7 mV, Fig. 4d. The long-term stable cycling of Li/LLZTO@LSO/Li symmetric cells points out desirable kinetic charge transfer and good Li-ion mobility at the interface of Li/LLZTO@LSO.

To validate the practicability of the LLZTO surface engineering technology, hybrid solid-state full cells were assembled with the LLZTO@LSO electrolyte, a kind of intercalation cathode $LiFePO_4$ (LFP) and lithium metal anode. The schematic diagram.

is shown in Fig. 5a. Fig. 5b show that the initial charge and discharge specific capacities are 140.4 and 127.6 mA h/g for the full cell at a current density of 50 μA cm^{-2}, respectively, with an initial coulombic efficiency of 90.8%. Moreover, the charge and discharge platforms are 3.47 V and 3.36 V, respectively, which display a small overpotential of 0.11 V. In addition, after 80 times cycling, the cell still maintains a specific capacity of 121.7 mA h/g with a capacity retention of 95%, showing excellent stability (Fig. 5c). Furthermore, as shown in Fig. 5d, we tested the rate performance of the full cell with the step increased current density at 50, 75, 100, and 150 μA cm^{-2}. The cell displays discharge capacities of 125.2, 122.1, 117.5, and 112.5 mA h/g, respectively. Moreover, the discharge capacities recover to 128.6 mA h/g after the current density drops to 50 μA cm^{-2}, showing good rate performance and reversibility. The favorable electrochemical performances of hybrid solid-state Li/LLZTO@LSO/LFP cells suggest the practicality of our surface engineering for enabling next-generation all-solid-state lithium batteries.

4. Conclusions

In summary, we proposed a novel approach to chemically upcycle the Li_2CO_3 impurities on the surface of the garnet electrolyte by transforming them into the LSO layer. Simultaneously, extra Li_2CO_3 is added to prevent the formation of Li-deficiency defects. The obtained LLZTO@LSO pellet displays perfect air stability because of the hydrophobic LSO. Meanwhile, LSO is confirmed to be lithiophilic. As a result, excellent wetting properties and well-contact interfaces for Li/LLZTO@LSO are achieved. Moreover, benefitting from the higher voltage stability and lithium-ion conductivity of the lithiophilic LSO than that of Li_2CO_3, the assembled Li/LLZTO@LSO/Li symmetric cell and Li/LLZTO@LSO/LFP hybrid solid-state full cell displays ultralow interfacial resistance, excellent rate performance, and perfect cycle reversibility and stability. We believe this novel "upcycling" idea could provide general insights to address the interface issue in SSLMBs. Meanwhile, it should be noted that supplying extra lithium is essential when eliminating the Li_2CO_3 from garnet.

CRediT authorship contribution statement

Jiaxu Zhang: Conceptualization, Methodology, Validation, Data analysis, Investigation, Writing – original draft. **Changhong Wang**: Conceptualization, Methodology, Validation, Data analysis, Investigation, Writing – review & editing. **Matthew Zheng**: Investigation, Writing – review & editing. **Minghao Ye**: Methodology, Data analysis. **Huiyu Zhai**: Methodology, Validation. **Jun Li**: Resource, Investigation. **Gangjian Tan**: Conceptualization, Methodology, Resources, Writing – review & editing, Supervision, Project administration. **Xinfeng Tang**: Resources, Writing – review & editing, Supervision. **Xueliang Sun**: Conceptualization, Writing – review & editing, Project administration,

Supervision.

Declaration of Competing Interest

The authors declare that they have no known competing financial interests or personal relationships that could have appeared to influence the work reported in this paper.

Data availability

Data will be made available on request.

Acknowledgments

We would like to acknowledge the financial support from the National Natural Science Foundation of China (Grant No. 11804261) and National Key Research and Development Program of China (Grant No. 2019YFA0704900).

Appendix A. Supporting information

Supplementary data associated with this article can be found in the online version at doi:10.1016/j.nanoen.2022.107672.

References

[1] L. Trahey, F.R. Brushett, N.P. Balsara, G. Ceder, L. Cheng, Y.-M. Chiang, N.T. Hahn, B.J. Ingram, S.D. Minteer, J.S. Moore, Energy storage emerging: a perspective from the Joint Center for Energy Storage Research, Proc. Natl. Acad. Sci. USA 117 (2020) 12550–12557.
[2] X.-B. Cheng, R. Zhang, C.-Z. Zhao, Q. Zhang, Toward safe lithium metal anode in rechargeable batteries: a review, Chem. Rev. 117 (2017) 10403–10473.
[3] D. Lin, Y. Liu, Y. Cui, Reviving the lithium metal anode for high-energy batteries, Nat. Nanotechnol. 12 (2017) 194.
[4] W. Xu, J. Wang, F. Ding, X. Chen, E. Nasybulin, Y. Zhang, J.-G. Zhang, Lithium metal anodes for rechargeable batteries, Energy Environ. Sci. 7 (2014) 513–537.
[5] Q. Yang, C. Li, Li metal batteries and solid state batteries benefiting from halogen-based strategies, Energy Storage Mater. 14 (2018) 100–117.
[6] D. Kang, N. Hart, J. Koh, L. Ma, W. Liang, J. Xu, S. Sardar, J.P. Lemmon, Rearrange SEI with artificial organic layer for stable lithium metal anode, Energy Storage Mater. 24 (2020) 618–625.
[7] Q. Yang, W. Li, C. Dong, Y. Ma, Y. Yin, Q. Wu, Z. Xu, W. Ma, C. Fan, K. Sun, PIM-1 as an artificial solid electrolyte interphase for stable lithium metal anode in high-performance batteries, J. Energy Chem. 42 (2020) 83–90.
[8] Z. Yu, H. Wang, X. Kong, W. Huang, Y. Tsao, D.G. Mackanic, K. Wang, X. Wang, W. Huang, S. Choudhury, Molecular design for electrolyte solvents enabling energy-dense and long-cycling lithium metal batteries, Nat. Energy 5 (2020) 526–533.
[9] J. Yi, J. Chen, Z. Yang, Y. Dai, W. Li, J. Cui, F. Ciucci, Z. Lu, C. Yang, Facile patterning of laser-induced graphene with tailored Li nucleation kinetics for stable lithium-metal batteries, Adv. Energy Mater. 9 (2019), 1901796.
[10] J. Janek, W.G. Zeier, A solid future for battery development, Nat. Energy 1 (2016) 1–4.
[11] M. Balaish, J.C. Gonzalez-Rosillo, K.J. Kim, Y.T. Zhu, Z.D. Hood, J.L.M. Rupp, Processing thin but robust electrolytes for solid-state batteries, Nat. Energy 6 (2021) 227–239.
[12] A.C. Kozen, A.J. Pearse, C.-F. Lin, M. Noked, G.W. Rubloff, Atomic layer deposition of the solid electrolyte LiPON, Chem. Mater. 27 (2015) 5324–5331.
[13] H.-P. Hong, Crystal structure and ionic conductivity of $Li_{14}Zn(GeO_4)_4$ and other new Li^+ superionic conductors, Mater. Res. Bull. 13 (1978) 117–124.
[14] K. Nanjundaswamy, A. Padhi, J. Goodenough, S. Okada, H. Ohtsuka, H. Arai, J. Yamaki, Synthesis, redox potential evaluation and electrochemical characteristics of NASICON-related-3D framework compounds, Solid State Ion. 92 (1996) 1–10.
[15] N. Anantharamulu, K.K. Rao, G. Rambabu, B.V. Kumar, V. Radha, M. Vithal, A wide-ranging review on Nasicon type materials, J. Mater. Sci. 46 (2011) 2821–2837.
[16] J.E. Trevey, Y.S. Jung, S.-H. Lee, High lithium ion conducting Li_2S–GeS_2–P_2S_5 glass–ceramic solid electrolyte with sulfur additive for all solid-state lithium secondary batteries, Electrochim. Acta 56 (2011) 4243–4247.
[17] X. Li, J. Liang, X. Yang, K.R. Adair, C. Wang, F. Zhao, X. Sun, Progress and perspectives on halide lithium conductors for all-solid-state lithium batteries, Energy Environ. Sci. 13 (2020) 1429–1461.
[18] R. Murugan, V. Thangadurai, W. Weppner, Fast lithium ion conduction in garnet-type $Li_7La_3Zr_2O_{12}$, Angew. Chem. Int. Ed. 46 (2007) 7778–7781.
[19] X. Yang, Q. Sun, C. Zhao, X. Gao, K.R. Adair, Y. Liu, J. Luo, X. Lin, J. Liang, H. Huang, L. Zhang, R. Yang, S. Lu, R. Li, X. Sun, High-areal-capacity all-solid-state lithium batteries enabled by rational design of fast ion transport channels in vertically-aligned composite polymer electrodes, Nano Energy 61 (2019) 567–575.
[20] L. Xu, J. Li, W. Deng, H. Shuai, S. Li, Z. Xu, J. Li, H. Hou, H. Peng, G. Zou, Garnet solid electrolyte for advanced all-solid-state Li batteries, Adv. Energy Mater. 10 (2020), 2000945.
[21] H. Huo, J. Luo, V. Thangadurai, X. Guo, C.-W. Nan, X. Sun, Li_2CO_3: a critical issue for developing solid garnet batteries, ACS Energy Lett. 5 (2020) 252–262.
[22] A. Sharafi, E. Kazyak, A.L. Davis, S. Yu, T. Thompson, D.J. Siegel, N.P. Dasgupta, J. Sakamoto, Surface chemistry mechanism of ultra-low interfacial resistance in the solid-state electrolyte $Li_7La_3Zr_2O_{12}$, Chem. Mater. 29 (2017) 7961–7968.
[23] C. Ma, E. Rangasamy, D.C. Liang, J. Sakamoto, K. More, M. Chi, Excellent stability of a lithium-ion-conducting solid electrolyte upon reversible Li, Angew. Chem. Int. Ed. 54 (2015) 129–133.
[24] L. Cheng, C.H. Wu, A. Jarry, W. Chen, Y. Ye, J. Zhu, R. Kostecki, K. Persson, J. Guo, M. Salmeron, G.Y. Chen, M. Doeff, Interrelationships among grain size, surface composition, air stability, and interfacial resistance of Al-substituted $Li_7La_3Zr_2O_{12}$ solid electrolytes, ACS Appl. Mater. Interfaces 7 (2015) 17649–17655.
[25] L. Cheng, E.J. Crumlin, W. Chen, R. Qiao, H. Hou, S.F. Lux, V. Zorba, R. Russo, R. Kostecki, Z. Liu, K. Persson, W. Yang, J. Cabana, T. Richardson, G. Chen, M. Doeff, The origin of high electrolyte-electrode interfacial resistances in lithium cells containing garnet type solid electrolytes, Phys. Chem. Chem. Phys. 16 (2014) 18294–18300.
[26] Y. Pang, J. Pan, J. Yang, S. Zheng, C. Wang, Electrolyte/electrode interfaces in all-solid-state lithium batteries: a review, Electrochem. Energy Rev. 4 (2021) 169–193.
[27] M. Jia, N. Zhao, H. Huo, X. Guo, Comprehensive investigation into garnet electrolytes toward application-oriented solid lithium batteries, Electrochem. Energy Rev. 3 (2020) 656–689.
[28] W. Luo, Y. Gong, Y. Zhu, Y. Li, Y. Yao, Y. Zhang, K. Fu, G. Pastel, C.F. Lin, Y. Mo, Reducing interfacial resistance between garnet-structured solid-state electrolyte and Li-metal anode by a germanium layer, Adv. Mater. 29 (2017), 1606042.
[29] K.K. Fu, Y. Gong, B. Liu, Y. Zhu, S. Xu, Y. Yao, W. Luo, C. Wang, S.D. Lacey, J. Dai, Toward garnet electrolyte–based Li metal batteries: An ultrathin, highly effective, artificial solid-state electrolyte/metallic Li interface, Sci. Adv. 3 (2017), e1601659.
[30] X. Han, Y. Gong, K.K. Fu, X. He, G.T. Hitz, J. Dai, A. Pearse, B. Liu, H. Wang, G. Rubloff, Negating interfacial impedance in garnet-based solid-state Li metal batteries, Nat. Mater. 16 (2017) 572.
[31] W. Luo, Y. Gong, Y. Zhu, K.K. Fu, J. Dai, S.D. Lacey, C. Wang, B. Liu, X. Han, Y. Mo, E.D. Wachsman, L. Hu, Transition from superlithiophobicity to superlithiophilicity of garnet solid-state electrolyte, J. Am. Chem. Soc. 138 (2016) 12258–12262.
[32] Y. Shao, H. Wang, Z. Gong, D. Wang, B. Zheng, J. Zhu, Y. Lu, Y.-S. Hu, X. Guo, H. Li, Drawing a soft interface: an effective interfacial modification strategy for garnet-type solid-state Li batteries, ACS Energy Lett. 3 (2018) 1212–1218.
[33] Y. Ren, Y. Shen, Y. Lin, C.-W. Nan, Direct observation of lithium dendrites inside garnet-type lithium-ion solid electrolyte, Electrochem. Commun. 57 (2015) 27–30.
[34] A.A. Delluva, J. Kulberg-Savercool, A. Holewinski, Decomposition of trace Li_2CO_3 during charging leads to cathode interface degradation with the solid electrolyte LLZO, Adv. Funct. Mater. 31 (2021), 2103716.
[35] C. Wang, H. Xie, W. Ping, J. Dai, G. Feng, Y. Yao, S. He, J. Weaver, H. Wang, K. Gaskell, A general, highly efficient, high temperature thermal pulse toward high performance solid state electrolyte, Energy Storage Mater. 17 (2019) 234–241.
[36] Y. Li, X. Chen, A. Dolocan, Z. Cui, S. Xin, L. Xue, H. Xu, K. Park, J.B. Goodenough, Garnet electrolyte with an ultralow interfacial resistance for Li-metal batteries, J. Am. Chem. Soc. 140 (2018) 6448–6455.
[37] H. Huo, Y. Chen, N. Zhao, X. Lin, J. Luo, X. Yang, Y. Liu, X. Guo, X. Sun, In-situ formed Li_2CO_3-free garnet/Li interface by rapid acid treatment for dendrite-free solid-state batteries, Nano Energy 61 (2019) 119–125.
[38] Y. Ruan, Y. Lu, X. Huang, J. Su, C. Sun, J. Jin, Z. Wen, Acid induced conversion towards a robust and lithiophilic interface for Li–$Li_7La_3Zr_2O_12$ solid-state batteries, J. Mater. Chem. A 7 (2019) 14565–14574.
[39] J. Zhang, R. Yu, J. Li, H. Zhai, G. Tan, X. Tang, Transformation of undesired Li_2CO_3 into lithiophilic layer via double replacement reaction for garnet electrolyte engineering, Energy Environ. Mater. in press. https://doi.org/10.1002/eem2.12222.
[40] H. Duan, W. Chen, M. Fan, W. Wang, L. Yu, S. Tan, X. Chen, Q. Zhang, S. Xin, L. Wan, Y. Guo, Building an air stable and lithium deposition regulable garnet interface from moderate-temperature conversion, Chem. Angew. Chem. Int. Ed. 59 (2020) 12069–12075.
[41] H.-K. Tian, B. Xu, Y. Qi, Computational study of lithium nucleation tendency in $Li_7La_3Zr_2O_{12}$ (LLZO) and rational design of interlayer materials to prevent lithium dendrites, J. Power Sources 392 (2018) 79–86.
[42] S. Wang, H. Xu, W. Li, A. Dolocan, A. Manthiram, Interfacial chemistry in solid-state batteries: formation of interphase and its consequences, J. Am. Chem. Soc. 140 (2018) 250–257.
[43] F.D. Han, A.S. Westover, J. Yue, X.L. Fan, F. Wang, M.F. Chi, D.N. Leonard, N. Dudney, H. Wang, C.S. Wang, High electronic conductivity as the origin of lithium dendrite formation within solid electrolytes, Nat. Energy 4 (2019) 187–196.
[44] J.-F. Wu, B.-W. Pu, D. Wang, S.-Q. Shi, N. Zhao, X. Guo, X. Guo, In situ formed shields enabling Li_2CO_3-free solid electrolytes: a new route to uncover the intrinsic lithiophilicity of garnet electrolytes for dendrite-free Li-metal batteries, ACS Appl. Mater. Interfaces 11 (2018) 898–905.
[45] E. Il'ina, K. Druzhinin, B. Antonov, A. Pankratov, E. Vovkotrub, Influence of Li_2O–Y_2O_3–SiO_2 glass additive on conductivity and stability of cubic $Li_7La_3Zr_2O_{12}$, Ionics 25 (2019) 5189–5199.

[46] N.C. Rosero-Navarro, T. Yamashita, A. Miura, M. Higuchi, K. Tadanaga, Effect of sintering additives on relative density and Li-ion conductivity of Nb-doped $Li_7La_3ZrO_{12}$ solid electrolyte, J. Am. Ceram. Soc. 100 (2017) 276–285.
[47] L. Cheng, M. Liu, A. Mehta, H. Xin, F. Lin, K. Persson, G. Chen, E.J. Crumlin, M. Doeff, Garnet electrolyte surface degradation and recovery, ACS Appl. Energy Mater. 1 (2018) 7244–7252.
[48] Y. Meesala, Y.-K. Liao, A. Jena, N.-H. Yang, W.K. Pang, S.-F. Hu, H. Chang, C.-E. Liu, S.-C. Liao, J.-M. Chen, An efficient multi-doping strategy to enhance Li-ion conductivity in the garnet-type solid electrolyte $Li_7La_3Zr_2O_{12}$, J. Mater. Chem. A 7 (2019) 8589–8601.
[49] P. Richet, B.O. Mysen, D. Andrault, Melting and premelting of silicates: Raman spectroscopy and X-ray diffraction of Li_2SiO_3 and Na_2SiO_3, Phys. Chem. Miner. 23 (1996) 157–172.
[50] O. Koroleva, M. Shtenberg, P. Khvorov, Vibrational spectroscopic and X-ray diffraction study of crystalline phases in the Li_2O-SiO_2 system, Russ. J. Inorg. Chem. 59 (2014) 255–258.
[51] N.C. Rosero-Navarro, R. Kajiura, R. Jalem, Y. Tateyama, A. Miura, K. Tadanaga, Significant reduction in the interfacial resistance of garnet-type solid electrolyte and lithium metal by a thick amorphous lithium silicate layer, ACS Appl. Energy Mater. 3 (2020) 5533–5541.
[52] R. Pfenninger, M. Struzik, I. Garbayo, E. Stilp, J.L.M. Rupp, A low ride on processing temperature for fast lithium conduction in garnet solid-state battery films, Nat. Energy 4 (2019) 475–483.